Letter

Interstate Berry curvature of hinge state and its detection

Zheng Liu,[1] Zhenhua Qiao,[1,2,*] Yang Gao,[1,2,†] and Qian Niu[1]

[1]*CAS Key Laboratory of Strongly-Coupled Quantum Matter Physics, and Department of Physics, University of Science and Technology of China, Hefei, Anhui 230026, China*

[2]*ICQD, Hefei National Laboratory for Physical Sciences at Microscale, University of Science and Technology of China, Hefei, Anhui 230026, China*

(Received 9 December 2022; revised 2 July 2023; accepted 13 December 2023; published 11 January 2024)

We demonstrate that the topological hinge state can possess a nontrivial interstate Berry curvature in the non-Abelian formulation of the Berry curvature. It can be readily probed by the circular photogalvanic effect (CPGE), with the light illuminating a specific hinge, and we refer to it as the hinge CPGE. As a concrete example, we calculate the hinge CPGE in ferromagnetic $MnBi_{2n}Te_{3n+1}$, and find that the hinge CPGE peak structure well reflects the interstate Berry curvature of hinge states and the optical sum rule captures the interstate Berry curvature between the hinge state and the ground state. Thus, the hinge CPGE provides a promising route towards the optical detection of a hinge-state geometrical structure.

DOI: 10.1103/PhysRevResearch.6.L012005

Recent years have witnessed a rapid development of higher-order topological insulators [1–24]. Different from first-order topological insulators, the higher-order topological insulator is characterized by topologically protected states that are at least two dimensions lower than their bulk states. For example, a three-dimensional second-order topological insulator can have topological conducting states localized on the hinges but not on the surfaces [6–16]. Therefore, probing hinge states is indispensable for understanding such a second-order topological insulator. By means of scanning tunneling microscopy [25–28], angle-resolved photoemission spectroscopy [29], and Josephson interference [25,30,31], the local density of states is resolved in both real and momentum space, suggesting the existence of hinge states. However, besides the characteristic spectrum information, it is still unclear whether the hinge state has any nontrivial geometrical structure and what are its consequences.

In this Letter, we demonstrate that a localized hinge state can have a non-Abelian Berry curvature component, which we refer to as the interstate Berry curvature. We then propose a hinge circular photogalvanic effect (CPGE) as a perfect probe of such an interstate Berry curvature of the hinge state. The CPGE refers to the part of the photocurrent that switches with the circular polarization of light [32], and is an efficient method for capturing the Berry curvature of bulk and surface states [33–44]. By additionally restricting the illuminating area to an appropriate region that fully encapsulates the hinge state spatially yet remains small compared to the sample size, one obtains the hinge CPGE (see Fig. 1). The hinge CPGE involves the interstate Berry curvature of the hinge state in a similar fashion with the CPGE and the corresponding sum rule measures the interstate Berry curvature between the hinge state and the ground state.

Using $MnBi_{2n}Te_{3n+1}$ as a concrete example, we numerically demonstrate the hinge CPGE and its detection of the interstate Berry curvature of hinge states. Specifically, we find that the photocurrent of hinge CPGE approaches a steady value as the sample size increases. It also exhibits peak structures due to the interstate Berry curvature of the hinge state. Furthermore, the optical sum rule indeed well reflects the interstate Berry curvature between the hinge state and the ground state. These properties make the hinge CPGE a promising candidate for detecting hinge-state geometrical structures.

Interstate Berry curvature of hinge states. We start with the Berry curvature in extended systems, which plays essential and increasing roles in solid state physics. For example, in the celebrated anomalous Hall effect, one encounters momentum space Berry curvature $\boldsymbol{\Omega}_n = \boldsymbol{\nabla}_{\boldsymbol{k}} \times \boldsymbol{a}_n(\boldsymbol{k})$, where n is the band index, $\boldsymbol{a}_n(\boldsymbol{k}) = \langle n\boldsymbol{k}|i\boldsymbol{\partial}_{\boldsymbol{k}}|n\boldsymbol{k}\rangle$ is the intraband Berry connection, and $|n\boldsymbol{k}\rangle = e^{-i\boldsymbol{k}\cdot\boldsymbol{r}}|\psi_{n\boldsymbol{k}}\rangle$ is the periodic part of the Bloch function. $\boldsymbol{\Omega}_n$ involves a single band index and is hence Abelian. The origin of such Berry curvature is the restriction of the position operator, $\tilde{r}_i = \hat{P}_n r_i \hat{P}_n$ with $P_n = \sum_{\boldsymbol{k}} |\psi_{n\boldsymbol{k}}\rangle\langle\psi_{n\boldsymbol{k}}|$ being the projection operator. The cross product of $\tilde{\boldsymbol{r}}$ then generates Abelian Berry curvature [45–47], $\boldsymbol{\Omega}^{ab} = -i\tilde{\boldsymbol{r}} \times \tilde{\boldsymbol{r}} = \sum_{\boldsymbol{k}} \boldsymbol{\Omega}_n(\boldsymbol{k})|\psi_{n\boldsymbol{k}}\rangle\langle\psi_{n\boldsymbol{k}}|$.

In optics, however, Abelian Berry curvature is not directly measurable and needs to be extended. A good example is the CPGE, where a photocurrent is induced by a circularly polarized light, according to

$$\frac{dJ_i}{dt} = \beta_{ij}(\omega)[i\boldsymbol{E}(\omega) \times \boldsymbol{E}^*(\omega)]_j, \tag{1}$$

with $\boldsymbol{E}(\omega)$ being the light electric field with frequency ω. The response function involves a different form of the Berry

*Corresponding author: qiao@ustc.edu.cn
†Corresponding author: ygao87@ustc.edu.cn

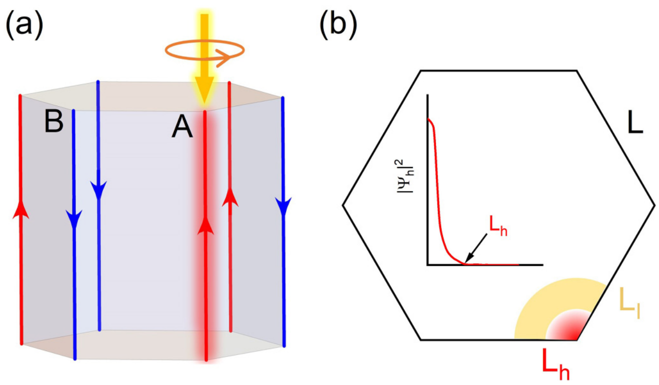

FIG. 1. (a) The hinge CPGE and (b) the corresponding top view of the hexagonal prism. In (a), the topological hinge states along hinges A and B are in red and blue, respectively. The photocurrent around hinge A with an illuminating area centered about the hinge is illustrated. In (b), the illuminated region and the localized hinge state are shown explicitly. It is required that $L_h \ll L_I \ll L$.

curvature [32]

$$\beta_{ij} = -\frac{\pi e^3}{\hbar V}\sum_{\boldsymbol{k},n,m} f_{nm}\Delta v_{i,nm}\left(\Omega_n^m\right)_j \delta(\hbar\omega - \omega_{mn}), \quad (2)$$

where $\omega_{mn} = \varepsilon_m - \varepsilon_n$ with ε_m being the band energy, $f_{nm} = f(\varepsilon_{nk}) - f(\varepsilon_{mk})$ with $f(\varepsilon_{nk})$ being the Fermi-Dirac distribution, $\Delta v_{i,nm} = \langle n|\hat{v}_i|n\rangle - \langle m|\hat{v}_i|m\rangle$ with $\hat{v}_i = \frac{1}{\hbar}\frac{\partial \hat{H}}{\partial k_i}$ being the velocity operator, and $\boldsymbol{\Omega}_n^m = -i\langle n\boldsymbol{k}|i\boldsymbol{\partial}|m\boldsymbol{k}\rangle \times \langle m\boldsymbol{k}|i\boldsymbol{\partial}|n\boldsymbol{k}\rangle$ is the geometrical factor.

Interestingly, $\boldsymbol{\Omega}_n^m$ is the difference between non-Abelian and Abelian Berry curvature. To see this, we define the projection operator onto a pair of bands n and m, $\hat{P} = \sum_{\boldsymbol{k}}(|\psi_{n\boldsymbol{k}}\rangle\langle\psi_{n\boldsymbol{k}}| + |\psi_{m\boldsymbol{k}}\rangle\langle\psi_{m\boldsymbol{k}}|)$. At each $\boldsymbol{k}$ point, one readily obtains a 2×2 non-Abelian Berry curvature, $\boldsymbol{\Omega}^{na} = -\frac{i}{2}\hat{e}_\ell\epsilon_{\ell ij}[\hat{P}r_i\hat{P}, \hat{P}r_j\hat{P}]$. The geometrical factor can then be expressed as $\boldsymbol{\Omega}_n^m = \langle\psi_{n\boldsymbol{k}}|\boldsymbol{\Omega}^{na} - \boldsymbol{\Omega}^{ab}|\psi_{n\boldsymbol{k}}\rangle$. The appearance of $\boldsymbol{\Omega}_n^m$ in optical phenomena such as the CPGE relies on two facts: First, the optical transition always relates two bands; second, $\boldsymbol{\Omega}_n^m$ is proportional to the oscillator strength of electron-circular-light coupling [48]. Given these features, we thus refer to $\boldsymbol{\Omega}_n^m$ as interband Berry curvature. It is invariant under the $U(1)$ gauge transformation of the eigenstate. We comment that besides interstate Berry curvature, one can also define the interstate quantum metric tensor, which is also essential in nonlinear optical phenomena [49].

The above interband Berry curvature can be readily generalized to be between a pair of states, including localized states. Here, we will focus on hinge states in three-dimensional second-order topological insulators. The generalization to other types of localized states (such as corner states) is straightforward. For this purpose, we consider a state pair formed by a hinge state and $|\psi_m\rangle$ and define $\hat{P} = |\psi_h\rangle\langle\psi_h| + |\psi_m\rangle\langle\psi_m|$. Using similar arguments as in periodic crystals, we have [46]

$$\begin{aligned}\Omega_h^m &= -i\langle\psi_h|[\hat{P}x\hat{P}, \hat{P}y\hat{P}]|\psi_h\rangle \\ &= -i\langle\psi_h|x|\psi_m\rangle\langle\psi_m|y|\psi_h\rangle - (x \leftrightarrow y). \quad (3)\end{aligned}$$

For localized states, interstate Berry curvature can be quite different from interband Berry curvature. For the latter, one can show that $\sum_m \Omega_n^m = \Omega_n$. In contrast, the localized hinge state does not have an Abelian Berry curvature. Assume the hinge state is localized in the x-O-y plane and define the projection operator as $\hat{P}_h = |\psi_h\rangle\langle\psi_h|$, with $|\psi_h\rangle$ labeling the hinge state. Since $|\psi_h\rangle$ is well localized, $\langle\psi_h|x|\psi_h\rangle$ and $\langle\psi_h|y|\psi_h\rangle$ are well defined. Then it is straightforward to prove that $[\hat{P}_h x\hat{P}_h, \hat{P}_h y\hat{P}_h] = 0$ identically. As a result, for interstate Berry curvature, we have $\sum_m \Omega_h^m = 0$. The interband Berry curvature usually appears in the study of bulk and surface states while its interstate counterpart will affect the response of the hinge state as discussed later [33–44].

Such interstate Berry curvature can be further generalized by expanding a single partner state to be a collection of states. This generalization is particularly useful in optics, as the optical sum rule generally relates to a continuum of states. To perform such a generalization, we use the ground-state projection operator,

$$\hat{P}_G = \sum_{m\in\text{occ}} |\psi_m\rangle\langle\psi_m|, \quad (4)$$

where occ stands for the collection of occupied states. By replacing the partner state projection $|\psi_m\rangle\langle\psi_m|$ with $\hat{P}_G$ in Eq. (3), we obtain

$$\Omega_h^G = -i\sum_{m\in occ}[\langle\psi_h|x|\psi_m\rangle\langle\psi_m|y|\psi_h\rangle] - (x \leftrightarrow y). \quad (5)$$

This is the interstate Berry curvature between the hinge state and the ground state of the topological material. We comment that since $[x, y] = 0$ identically, the Berry curvature between the hinge state and occupied states differs by a sign from that between the hinge state and unoccupied states. Such Berry curvature Ω_h^G is a consequence of higher-order band topology [47].

Hinge CPGE. Strikingly, such interstate Berry curvature can be readily probed using a variant of the CPGE. The difficulty of optically probing the edge state is the isolation of its contribution from the bulk contribution. This can be realized by using different symmetry constraints on the edge and bulk, as proposed in Refs. [50,51]. Here, we propose another method by fine tuning the illuminating area. Without loss of generality, we consider a sample that is finite in the xy plane and periodic along the z direction. We then assume a circularly polarized light propagating along the z direction with an illuminating region labeled by I. To probe the hinge state, we further require that the characteristic length scale for the hinge state (L_h), illuminating area (L_I), and the sample (L) satisfies $L_h \ll L_I \ll L$, as shown in Fig. 1. They do not need to be compared with the length scale along the zth direction. We focus on the induced photocurrent along the zth direction and in the same region I (different from the in-plane photocurrent in the study of the surface state [39,50]). The corresponding response coefficient reads [47]

$$\begin{aligned}\beta_{zz}^h(\omega) = &-\frac{e^3}{2\hbar}\int dk_z \sum_{n,m}^{a\in I} f_{nm}[\langle n|(\hat{v}_z)_a|n\rangle - \langle m|(\hat{v}_z)_a|m\rangle] \\ &\times \left(\Omega_n^m\right)^I \delta(\hbar\omega - \omega_{mn}), \quad (6)\end{aligned}$$

where $(\hat{v}_z)_a = \{\hat{v}_z, \hat{P}_a\}/2$ projects the velocity on site a, and $\hat{P}_a$ is the projection operator with the property $\sum_a \hat{P}_a = 1$. The

TABLE I. The scaling properties of various factors in β_{zz} due to different optical excitation processes.

Processes	$h \leftrightarrow h$	$h \leftrightarrow s$	$h \leftrightarrow b$	$s \leftrightarrow s$	$s \leftrightarrow b$	$b \leftrightarrow b$
$\sum_{a\in I}(\Delta v_z)_a$	$O(1)$	$O(1)$	$O(1)$	$O(L_I/L)$	$O(L_I/L)$	$O(L_I^2/L^2)$
Ω_n^m	$O(1)$	$O(1/L)$	$O(1/L^2)$	$O(L_I^2/L^2)$	$O(L_I^2/L^3)$	$O(L_I^4/L^4)$
Multiplicity	$O(1)$	$O(L)$	$O(L^2)$	$O(L)$	$O(L^2)$	$O(L^2)$
β_{zz}^h	$O(1)$	$O(1)$	$O(1)$	$O(L_I^3/L^2)$	$O(L_I^3/L^2)$	$O(L_I^6/L^4)$

geometric factor is given by

$$\left(\Omega_n^m\right)^I = \langle n|i[\tilde{x}^I, \tilde{y}^I]|n\rangle, \tag{7}$$

where $\tilde{r}_i^I = \hat{P}\hat{P}_I r_i \hat{P}_I \hat{P}$ with $\hat{P}_I = \sum_{a\in I}\hat{P}_a$ projects onto the illuminating region. It differs from interstate Berry curvature as an additional spatial projection due to a restricted illumination area is needed. We refer to such a photocurrent with a restricted illuminating area over one hinge as the hinge CPGE.

Due to the length-scale requirement, β_{zz}^h is a thermodynamic property of the sample that only involves the hinge-state properties. To prove this, we first note that there are three sets of bands in the sample: a bulk band, surface band, and hinge band. An incident light with an arbitrary frequency can generally excite electrons within these bands, i.e., there are nine different types of contributions. However, different contributions scale differently with the sample size according to the localized nature of different states. Take the hinge-to-surface or surface-to-hinge process ($h \leftrightarrow s$) as an example. For site a at the hinge, $\langle a|n\rangle \sim O(1)$ if $|n\rangle$ belongs to the hinge states, while $\langle a|n\rangle \sim O(1/\sqrt{L})$ if $|n\rangle$ belongs to the surface states. The resulting velocity factor in Eq. (6) satisfies $\langle n|(v_z)_a|n\rangle \sim O(1)$ for hinge states while $\langle n|(v_z)_a|n\rangle \sim O(1/L)$ for surface states. By using similar arguments, we find that the scaling behavior of the geometrical factor $(\Omega_n^m)^I \sim O(1/L)$.

Besides the obvious velocity and geometrical factor, the summation over n and m brings additional multiplicity. With increasing sample size, the number of hinge and surface states scale as $O(1)$ and $O(L)$, respectively. Therefore, the summation over the hinge-surface band pair adds an $O(L)$ factor. Putting all these factors together, we find that the $h \leftrightarrow s$ process scales as $O(1)$ in the thermodynamic limit, i.e., it survives and behaves as a thermodynamic property of the sample.

Using similar arguments, we systematically studied the scaling behavior of the remaining processes. Details are given in the Supplemental Material [47] and the result is summarized in Table I. It is readily found that in the thermodynamic limit, only the contributions involving the hinge state (e.g., $h \leftrightarrow h$, $h \leftrightarrow s$, and $h \leftrightarrow b$) survive while all the others vanish. The response function can then be put in compact form as

$$\beta_{zz}^h(\omega) = -\frac{e^3}{2\hbar}\int dk_z \sum_m^{n\in H} f_{nm}(v_z)_n \Omega_n^m G_{nm}, \tag{8}$$

where H represents the set of hinge bands near the illuminated hinge, and $G_{nm} = \delta(\hbar\omega - \omega_{mn}) - \delta(\hbar\omega + \omega_{mn})$ accounts for the energy conservation. The geometrical factor Ω_n^m no longer involves the real-space projection: It reduces to interstate Berry curvature for the hinge state introduced previously. Similar to the discussion of Eq. (2), we expect Ω_n^m to appear in the response of the hinge state to circular light. Equation (8) explicitly shows that the hinge CPGE can probe the interstate Berry curvature of hinge states.

The interstate Berry curvature Ω_n^m between the hinge state and the ground state can be further extracted using the optical sum rule. To show this, we sum the response function over frequency and define

$$\Gamma_h = \int_0^{+\infty} \beta_{zz}^h(\omega)d\omega. \tag{9}$$

At finite temperature, the result reads [47]

$$\Gamma_h = -\frac{e^3}{2\hbar}\int dk_z \sum_{n\in H}(v_z)_n \Omega_n^G(1-2f_n), \tag{10}$$

where f_n is the Fermi function at finite temperature. The sum rule in Eq. (10) then involves the interstate Berry curvature between the hinge state and the ground state.

Demonstration in $MnBi_{2n}Te_{3n+1}$. As a concrete example, we now demonstrate the interstate Berry curvature and hinge CPGE in $MnBi_{2n}Te_{3n+1}$. We focus on the ferromagnetic state of $MnBi_{2n}Te_{3n+1}$, which is predicted to be a three-dimensional second-order topological insulator [13]. In the absence of magnetization, the point group of $MnBi_{2n}Te_{3n+1}$ is D_{3d} with the following generators: the spatial inversion I, threefold rotation around z axis C_{3z}, and twofold rotation around x axis C_{2x}. When magnetization is introduced, I and C_{3z} are preserved but C_{2x} is replaced by $C_{2x}T$. The inversion symmetry forbids the bulk CPGE. For each surface, the inversion symmetry is absent but M_xT symmetry remains, forbidding the net photocurrent on the surface. Each hinge further breaks M_xT and preserves only $C_{2x}T$ symmetry, hence permitting the hinge CPGE. The lattice structure, symmetry operations, and the model Hamiltonian are included in the Supplemental Material [47].

To calculate the hinge CPGE, we consider a hexagonal prism geometry that is periodic in the z direction. The side length is set as $L = 16a_0$ with a_0 representing the lattice constant. The corresponding energy spectrum is shown in Fig. 2(a). We find gapless hinge states between the gapped surface states.

We first calculate the injection current at the hinge as well as over the surface and bulk with the whole sample illuminated [47]. We find that it is nonzero at the hinge but vanishes in the bulk and surface β_{zz}, consistent with the symmetry analysis. The β_{zz} has the same form of Eq. (6), but changes the summation of the atomic site a to the desired region. The nontrivial injection current at the hinge with the light energy below the surface band gap signifies the existence of a hinge state. To illustrate such an injection current, we plot $\beta_{zz}(\omega)$ at a lattice site a with $\hbar\omega/t = 0.24$ in Fig. 2(b). One immediately finds that β_{zz} is highly localized around the six hinges, with

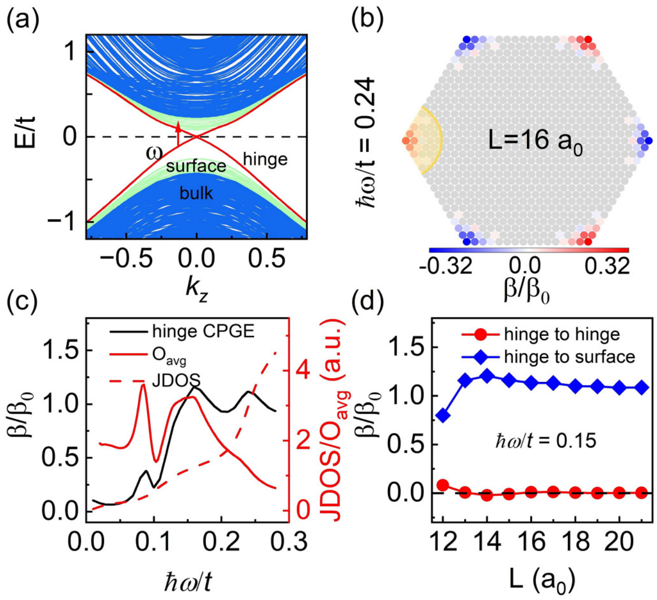

FIG. 2. (a) The band structure of $MnBi_{2n}Te_{3n+1}$ with size $L = 16a_0$. The hinge, surface, and bulk states are in red, cyan, and blue, respectively. (b) The distribution of $\beta_{zz}(\omega, a)$ in the xy plane at $\hbar\omega/t = 0.24$. (c) The hinge CPGE coefficient, the joint density of states, and average interstate Berry curvature as a function of frequency. $\beta_0 = \pi^3 e^3/h^2$. (d) The hinge to hinge and hinge to surface contribution to β^h_{zz} as a function of sample size with $\hbar\omega/t = 0.15$. The illuminating region is illustrated in yellow in (b).

an alternating pattern due to the D_{3d} point group of the whole sample.

We then focus on the left hinge and calculate β^h_{zz} corresponding to the hinge CPGE by restricting the illuminating area to be near that hinge. The frequency dependence is shown in Fig. 2(c). When the light energy is below $0.08t$, the electron can be excited from one hinge state to another, while above $0.08t$, the electron can be excited additionally to the surface state. Since more electronic states are involved, one observes a roughly synchronized trend of increase between the hinge CPGE coefficient and the joint density of states, with the latter defined as follows,

$$\mathrm{JDOS} = \sum_{m,n} \int \frac{dk_z}{2\pi} f_{nm} \delta(\hbar\omega - \omega_{mn}). \tag{11}$$

On top of the synchronized increase trend, the response coefficient shows additional peak structures, which is the manifestation of the interstate Berry curvature. Based on Eq. (6), we can define $O(\omega) = \sum_{n,m} \int \frac{dk_z}{2\pi} f_{nm} \Omega^m_n \delta(\hbar\omega - \omega_{mn})$. It has a clear physical meaning: $\omega^2 O(\omega)$ is just the difference of the absorption rate between the left and right circularly polarized lights [48,52]. Then, we get the average interstate Berry curvature $O_{\mathrm{avg}}(\omega) = O(\omega)/\mathrm{JDOS}(\omega)$ and plot it in Fig. 2(c). One immediately finds that peaks in β^h_{zz} are related to that of $O_{\mathrm{avg}}(\omega)$, clearly demonstrating the essential role of the interstate Berry curvature.

To clarify the scaling property of hinge CPGE, we choose $\hbar\omega/t = 0.15$ and two transition processes contribute to the injection current: $h \leftrightarrow h$ and $h \leftrightarrow s$. In Fig. 2(d), we plot these two contributions against the sample size. One observes

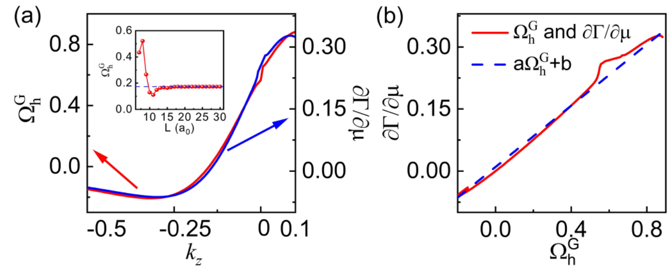

FIG. 3. (a) The hinge-state Berry curvature (in units of a_0^2) and $\partial\Gamma/\partial\mu$ (in units of $a_0^2 e^3/\hbar$) as a function of k_z. The sample size is $L = 16a_0$. The inset shows the Berry curvature at $k_z = -0.1$ for different sample sizes. Here, we represent $\partial\Gamma/\partial\mu$ as a function of k_z as each chemical potential corresponds to a unique lattice momentum for the hinge state. (b) The relationship between the sum rule and the hinge-state Berry curvature obtained by the least-squares fitting. The parameters a and b are 0.37 and 0.01, respectively.

that the $h \leftrightarrow h$ contribution gradually vanishes as the two hinges are spatially separated in $MnBi_{2n}Te_{3n+1}$. In contrast, the $h \leftrightarrow s$ contribution reaches a steady value, irrelevant with the sample size and consistent with the previous analysis.

Finally, to illustrate the relation between the optical sum rule and the hinge-state Berry curvature, we compare the interstate Berry curvature for the hinge state and the results from the sum rule. At zero temperature, utilizing the properties of the δ function, we prove that they have the following dependence [47]:

$$\frac{\partial\Gamma_h}{\partial\mu} = \frac{e^3}{\hbar}\int dk_z \sum_{n\in H} (v_z)_n \Omega^G_n \frac{\partial f_n}{\partial\mu}$$
$$\underline{\underline{T\to 0}}\ \frac{e^3}{\hbar}\sum_{n\in H}^{\varepsilon_n=\mu} \mathrm{sgn}[(v_z)_n]\Omega^G_n(k_F). \tag{12}$$

Therefore, the variation of the sum rule directly measures the Berry curvature at the Fermi momentum, weighted by the sign of the Fermi velocity. By changing the doping level, the hinge-state Berry curvature then can be mapped across the Brillouin zone. At finite temperature, the optical sum rule is smeared by contributions at the energy range of $k_B T$ and hence the linear dependence is compromised [47].

To numerically demonstrate such a linear dependence, in Fig. 3(a) we calculate the optical sum rule and the interstate Berry curvature. We find that the linear fitting agrees well with the data. In addition, the constant term b approaches zero, consistent with Eq. (12). Moreover, we note that due to D_{3d} symmetry, the contribution from the three hinges connected by C_3 symmetry is the same. Since we are calculating the photocurrent along one hinge in Fig. 3, we should have $a = e^3/(3\hbar)$. This is consistent with the fitting value 0.37. Therefore, the connection between the optical sum rule and the interstate Berry curvature is well exemplified.

In summary, we have generalized the bulk Berry curvature to the interstate Berry curvature for the hinge state, and proposed the hinge CPGE as a prefect probe for it. Using the ferromagnetic state of $MnBi_{2n}Te_{3n+1}$ as an example, we demonstrate the unique properties of the hinge CPGE. Our results demonstrate the important role of the Berry curvature of the hinge state and call for future studies to further explore other geometrical quantities of the hinge state and their transport and optical implications.

Acknowledgments. Y.G. is supported by the National Key R&D Program under Grant No. 2022YFA1403502, National Natural Science Foundation of China (Grant No. 12374164), and Fundamental Research Funds for the Central Universities (Grant No. WK2340000102). Z.L. and Z.Q. are supported by the National Natural Science Foundation of China (11974327 and 12004369), Fundamental Research Funds for the Central Universities (WK3510000010, WK2030020032), Anhui Initiative in Quantum Information Technologies (No. AHY170000), and Innovation Program for Quantum Science and Technology (2021ZD0302800). Z.L. is also supported by the Postdoctoral Support Program (GZC20232562). Q.N. is supported by the National Natural Science Foundation of China (12234017). The supercomputing service of USTC is gratefully acknowledged.

[1] W. A. Benalcazar, B. A. Bernevig, and T. L. Hughes, Quantized electric multipole insulators, Science **357**, 61 (2017).

[2] W. A. Benalcazar, B. A. Bernevig, and T. L. Hughes, Electric multipole moments, topological multipole moment pumping, and chiral hinge states in crystalline insulators, Phys. Rev. B **96**, 245115 (2017).

[3] F. Zhang, C. L. Kane, and E. J. Mele, Surface state magnetization and chiral edge states on topological insulators, Phys. Rev. Lett. **110**, 046404 (2013).

[4] M. Ezawa, Higher-order topological insulators and semimetals on the breathing kagome and pyrochlore lattices, Phys. Rev. Lett. **120**, 026801 (2018).

[5] R. Chen, C. Z. Chen, J. H. Gao, B. Zhou, and D. H. Xu, Higher-order topological insulators in quasicrystals, Phys. Rev. Lett. **124**, 036803 (2020).

[6] M. Geier, L. Trifunovic, M. Hoskam, and P. W. Brouwer, Second-order topological insulators and superconductors with an order-two crystalline symmetry, Phys. Rev. B **97**, 205135 (2018).

[7] F. Schindler, A. M. Cook, M. G. Vergniory, Z. Wang, S. S. P. Parkin, B. A. Bernevig, and T. Neupert, Higher-order topological insulators, Sci. Adv. **4**, eaat0346 (2018).

[8] J. Langbehn, Y. Peng, L. Trifunovic, F. von Oppen, and P. W. Brouwer, Reflection-symmetric second-order topological insulators and superconductors, Phys. Rev. Lett. **119**, 246401 (2017).

[9] Z. Song, Z. Fang, and C. Fang, $(d-2)$-dimensional edge states of rotation symmetry protected topological states, Phys. Rev. Lett. **119**, 246402 (2017).

[10] F. Liu, H. Y. Deng, and K. Wakabayashi, Helical topological edge states in a quadrupole phase, Phys. Rev. Lett. **122**, 086804 (2019).

[11] D. Călugăru, V. Juričić, and B. Roy, Higher-order topological phases: A general principle of construction, Phys. Rev. B **99**, 041301(R) (2019).

[12] L. Trifunovic and P. W. Brouwer, Higher-order bulk-boundary correspondence for topological crystalline phases, Phys. Rev. X **9**, 011012 (2019).

[13] R. X. Zhang, F. Wu, and S. Das Sarma, Mobius insulator and higher-order topology in $MnBi_{2n}Te_{3n+1}$, Phys. Rev. Lett. **124**, 136407 (2020).

[14] Z. Wang, B. J. Wieder, J. Li, B. Yan, and B. A. Bernevig, Higher-order topology, monopole nodal lines, and the origin of large Fermi arcs in transition metal dichalcogenides XTe$_2$ ($X =$ Mo, W), Phys. Rev. Lett. **123**, 186401 (2019).

[15] Y. Xu, Z. Song, Z. Wang, H. Weng, and X. Dai, Higher-order topology of the axion insulator $EuIn_2As_2$, Phys. Rev. Lett. **122**, 256402 (2019).

[16] C. Yue, Y. Xu, Z. Song, H. Weng, Y. Lu, C. Fang, and X. Dai, Symmetry-enforced chiral hinge states and surface quantum anomalous Hall effect in the magnetic axion insulator $Bi_{2-x}Sm_xSe_3$, Nat. Phys. **15**, 577 (2019).

[17] K. Kudo, T. Yoshida, and Y. Hatsugai, Higher-order topological Mott insulators, Phys. Rev. Lett. **123**, 196402 (2019).

[18] Y. Ren, Z. Qiao, and Q. Niu, Engineering corner states from two-dimensional topological insulators, Phys. Rev. Lett. **124**, 166804 (2020).

[19] X. L. Sheng, C. Chen, H. Liu, Z. Chen, Z. M. Yu, Y. X. Zhao, and S. A. Yang, Two-dimensional second-order topological insulator in graphdiyne, Phys. Rev. Lett. **123**, 256402 (2019).

[20] M. J. Park, Y. Kim, G. Y. Cho, and S. B. Lee, Higher-order topological insulator in twisted bilayer graphene, Phys. Rev. Lett. **123**, 216803 (2019).

[21] B. Liu, L. Xian, H. Mu, G. Zhao, Z. Liu, A. Rubio, and Z. F. Wang, Higher-order band topology in twisted moiré superlattice, Phys. Rev. Lett. **126**, 066401 (2021).

[22] C. Cong, Z. Song, J. Zhao, Z. Chen, Z. Yu, X. Sheng, and S. A. Yang, Universal approach to magnetic second-order topological insulator, Phys. Rev. Lett. **125**, 056402 (2020).

[23] O. Pozo, C. Repellin, and A. G. Grushin, Quantization in chiral higher order topological insulators: Circular dichroism and local Chern marker, Phys. Rev. Lett. **123**, 247401 (2019).

[24] B. Xie, H. Wang, X. Zhang, P. Zhan, J. Jiang, M. Lu, and Y. Chen, Higher-order band topology, Nat. Rev. Phys. **3**, 520 (2021).

[25] F. Schindler, Z. Wang, M. G. Vergniory, A. M. Cook, A. Murani, S. Sengupta, A. Y. Kasumov, R. Deblock, S. Jeon, L. Drozdov, H. Bouchiat, S. Guéron, A. Yazdani, B. A. Bernevig, and T. Neupert, Higher-order topology in bismuth, Nat. Phys. **14**, 918 (2018).

[26] B. Jäck, Y. Xie, J. Li, S. Jeon, B. A. Bernevig, and A. Yazdani, Observation of a Majorana zero mode in a topologically protected edge channel, Science **364**, 1255 (2019).

[27] N. Shumiya, M. S. Hossain, J. Yin, Z. Wang, M. Litskevich, C. Yoon, Y. Li, Y. Yang, Y. Jiang, G. Cheng, Y. Lin, Q. Zhang, Z. Cheng, T. A. Cochran, D. Multer, X. P. Yang, B. Casas, T. Chang, T. Neupert, Z. Yuan *et al.*, Evidence of a room-temperature quantum spin Hall edge state in a higher-order topological insulator, Nat. Mater. **21**, 1111 (2022).

[28] L. Aggarwal, P. Zhu, T. L. Hughea, and V. Madhavan, Evidence for higher order topology in Bi and $Bi_{0.92}Sb_{0.08}$, Nat. Commun. **12**, 4420 (2021).

[29] R. Noguchi, M. Kobayashi, Z. Jiang, K. Kuroda, T. Takahashi, Z. Xu, D. Lee, M. Hirayama, M. Ochi, T. Shirasawa, P. Zhang, C. Lin, C. Bareille, S. Sakuragi, H. Tanaka, S. Kunisada, K. Kurokawa, K. Yaji, A. Harasawa, V. Kandyba *et al.*, Evidence for a higher-order topological insulator in a three-dimensional material built from van der Waals stacking of bismuth-halide chains, Nat. Mater. **20**, 473 (2021).

[30] A. Murani, A. Kasumov, S. Sengupta, Y. A. Kasumov, V. T. Volkov, I. I. Khodos, F. Brisset, R. Delagrange, A. Chepelianskii, R. Deblock, H. Bouchiat, and S. Guéron, Ballistic edge states in Bismuth nanowires revealed by SQUID interferometry, Nat. Commun. **8**, 15941 (2017).

[31] Y. Choi, Y. Xie, C. Chen, J. Park, S. Song, J. Yoon, B. J. Kim, T. Taniguchi, K. Watanabe, J. Kim, K. C. Fong, M. N. Ali, K. T. Law, and G. Lee, Evidence of higher-order topology in multilayer WTe_2 from Josephson coupling through anisotropic hinge states, Nat. Mater. **19**, 974 (2020).

[32] J. E. Sipe and A. I. Shkrebtii, Calculation of second-order optical response in semiconductors, Phys. Rev. B **61**, 5337 (2000).

[33] T. Morimoto, S. Zhong, J. Orenstein, and J. E. Moore, Semiclassical theory of nonlinear magneto-optical responses with applications to topological Dirac/Weyl semimetals, Phys. Rev. B **94**, 245121 (2016).

[34] F. de Juan, A. G. Grushin, T. Morimoto, and J. E. Moore, Quantized circular photogalvanic effect in Weyl semimetals, Nat. Commun. **8**, 15995 (2017).

[35] A. Avdoshkin, V. Kozii, and J. E. Moore, Interactions remove the quantization of the chiral photocurrent at Weyl points, Phys. Rev. Lett. **124**, 196603 (2020).

[36] J. E. Moore and J. Orenstein, Confinement-induced Berry phase and helicity-dependent photocurrents, Phys. Rev. Lett. **105**, 026805 (2010).

[37] E. Deyo, L. E. Golub, E. L. Ivchenko, and B. Spivak, Semiclassical theory of the photogalvanic effect in non-centrosymmetric systems, arXiv:0904.1917.

[38] Q. Ma, S. Xu, C. Chan, C. Zhang, G. Chang, Y. Lin, W. Xie, T. Palacios, H. Lin, S. Jia, P. A. Lee, P. Jarillo-Herrero, and N. Gedik, Direct optical detection of Weyl fermion chirality in a topological semimetal, Nat. Phys. **13**, 842 (2017).

[39] P. Hosur, Circular photogalvanic effect on topological insulator surfaces: Berry-curvature-dependent response, Phys. Rev. B **83**, 035309 (2011).

[40] F. Flicker, F. de Juan, B. Bradlyn, T. Morimoto, M. G. Vergniory, and A. G. Grushin, Chiral optical response of multifold fermions, Phys. Rev. B **98**, 155145 (2018).

[41] S. Xu, Q. Ma, H. Shen, V. Fatemi, S. Wu, T. Chang, G. Chang, A. M. Mier Valdivia, C. Chan, Q. D. Gibson, J. Zhou, Z. Liu, K. Watanabe, T. Taniguchi, H. Lin, R. J. Cava, L. Fu, N. Gedik, and P. Jarillo-Herrero, Electrically switchable Berry curvature dipole in the monolayer topological insulator WTe_2, Nat. Phys. **14**, 900 (2018).

[42] T. Holder, D. Kaplan, and B. Yan, Consequences of time-reversal-symmetry breaking in the light-matter interaction: Berry curvature, quantum metric, and diabatic motion, Phys. Rev. Res. **2**, 033100 (2020).

[43] J. Ahn, G. Y. Guo, and N. Nagaosa, Low-frequency divergence and quantum geometry of the bulk photovoltaic effect in topological semimetals, Phys. Rev. X **10**, 041041 (2020).

[44] D. Rees, K. Manna, B. Lu, T. Morimoto, H. Borrmann, C. Felser, J. E. Moore, D. H. Torchinsky, and J. Orenstein, Helicity-dependent photocurrents in the chiral Weyl semimetal RhSi, Sci. Adv. **6**, eaba0509 (2020).

[45] D. Xiao, M. C. Chang, and Q. Niu, Berry phase effects on electronic properties, Rev. Mod. Phys. **82**, 1959 (2010).

[46] R. Bianco and R. Resta, Mapping topological order in coordinate space, Phys. Rev. B **84**, 241106(R) (2011).

[47] See Supplemental Material at http://link.aps.org/supplemental/10.1103/PhysRevResearch.6.L012005 for the equation of Berry curvature in periodic crystal, derivations of response function, scaling properties, and sum rule of hinge CPGE, the lattice, symmetry, and the Hamiltonian of ferromagnetic $MnBi_{2n}Te_{3n+1}$, the illustrations of photocurrent and symmetry properties related to hinge CPGE, the microscopic origin of the peak structures in hinge CPGE, the temperature influence, and the topological feature of hinge state Berry curvature, which includes Refs. [53,54].

[48] I. Souza and D. Vanderbilt, Dichroic f-sum rule and the orbital magnetization of crystals, Phys. Rev. B **77**, 054438 (2008).

[49] J. Ahn, G. Guo, N. Nagaosa, and A. Vishwanath, Riemannian geometry of resonant optical responses, Nat. Phys. **18**, 290 (2022).

[50] G. Chang, J. X. Yin, T. Neupert, D. S. Sanchez, I. Belopolski, S. S. Zhang, T. A. Cochran, Z. Chéng, M. C. Hsu, S. M. Huang, B. Lian, S. Y. Xu, H. Lin, and M. Z. Hasan, Unconventional photocurrents from surface Fermi arcs in topological chiral semimetals, Phys. Rev. Lett. **124**, 166404 (2020).

[51] D. Rees, B. Lu, Y. Sun, K. Manna, R. Özgür, S. Subedi, H. Borrmann, C. Felser, J. Orenstein, and D. H. Torchinsky, Direct measurement of helicoid surface states in RhSi using nonlinear optics, Phys. Rev. Lett. **127**, 157405 (2021).

[52] Y. Gao, Y. Zhang, and D. Xiao, Tunable layer circular photogalvanic effect in twisted bilayers, Phys. Rev. Lett. **124**, 077401 (2020).

[53] E. I. Blount, in *Solid State Physics*, edited by F. Seitz and D. Turnbull (Academic Press, New York, 1962), Vol. 13, p. 305.

[54] C. X. Liu, X. L. Qi, H. J. Zhang, X. Dai, Z. Fang, and S. C. Zhang, Model Hamiltonian for topological insulators, Phys. Rev. B **82**, 045122 (2010).